ACCOUNTS of chemical research

pubs.acs.org/accounts Article

Combustion Synthesis and Polymer Doping of Metal Oxides for High-Performance Electronic Circuitry

Binghao Wang,[†] Wei Huang,[†] Michael J. Bedzyk, Vinayak P. Dravid, Yan-Yan Hu, Tobin J. Marks,* and Antonio Facchetti*

Cite This: *Acc. Chem. Res.* 2022, 55, 429−441 Read Online

ACCESS | Metrics & More | Article Recommendations

CONSPECTUS: Transparent conducting oxides (TCOs) are inorganic electrical conductors with optical band gaps greater than 3.3 eV. TCOs have been extensively explored in functional windows, touch screen applications, transparent displays, solar cells, and even electronic circuits. Amorphous metal oxide (a-MO) semiconductors are a TCO class that has made impressive progress since the first 2004 demonstration of their utility as the semiconducting layer in thin-film transistors (TFTs). Their excellent counterintuitive electron mobilities in the amorphous state fill the performance gap between amorphous silicon and polysilicon, widening TFT applicability to high-value products such as high-resolution flat panel displays and emerging flexible/wearable electronics. The possibility of solution processing MO "inks" from air-stable precursors, via roll-to-roll and high-throughput printing, further expands their appeal. However, most MO TFTs fabricated using solution-processing require postdeposition film annealing at elevated temperatures (>400 °C) to ensure high-quality films and stable charge transport. Thus, MO fabrication on and TFT integration with inexpensive and typically temperature-sensitive flexible polymer substrates remains challenging, as does reducing MO processing times to those acceptable for high-throughput semiconductor circuit manufacture. Consequently, new MO film processing methodologies are being developed to meet these requirements. Among them, science-based combustion synthesis (CS) and polymer doping are promising complementary approaches to optimize materials quality and manufacturing efficiency; they are the topic of this Account.

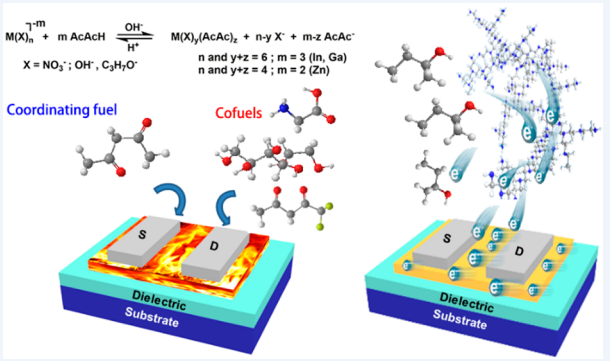

This Account summarizes the progress in CS and MO polymer doping research, made largely at Northwestern University over the past decade, to create high-performance MO TFTs. Regarding CS, we begin with an overview of combustion precursor chemistry that strongly affects the resulting film quality and device performance. Then, single fuel and dual fuel combustion syntheses for diverse MO systems are discussed. Representative examples highlight recent advances, with a focus on the relationship between (co)fuel-oxidizer types/amounts, thermal behavior, film microstructure, and TFT performance. Next, the discussion focuses on polymer doping of several MO matrices as a new approach to achieve semiconducting MO compositions with excellent performance and mechanical flexibility. Thus, the effect of the polymer architecture and content in the MO precursor formulations on the MO film composition, microstructure, electronic structure, and charge transport are discussed. The concluding remarks highlight challenges and emerging opportunities.

KEY REFERENCES

- Kim, M. G.; Kanatzidis, M. G.; Facchetti, A.; Marks, T. J. Low-temperature fabrication of high-performance metal oxide thin-film electronics via combustion processing. *Nat Mater.* **2011**, *10*, 382−388.[1] *The first report of combustion processing as a new general route to solution growth of diverse electronic metal oxide films at temperatures as low as 200 °C.*
- Yu, X.; Smith, J.; Zhou, N. J.; Zeng, L.; Guo, P. J.; Xia, Y.; Alvarez, A.; Aghion, S.; Lin, H.; Yu, J. S.; Chang, R. P. H.; Bedzyk, M. J.; Ferragut, R.; Marks, T. J.; Facchetti, A. Spray-combustion synthesis: Efficient solution route to high-performance oxide transistors. *Proc. Natl. Acad. Sci. USA* **2015**, *112*, 3217−3222.[2] *Reports a conformal, large-area coating technique, spray-combustion synthesis, and demonstrates IGZO semiconductor film thickness, densification, nanoporosity, electron mobility, trap densities,*

Received: October 27, 2021
Published: January 19, 2022

https://doi.org/10.1021/acs.accounts.1c00671
Acc. Chem. Res. 2022, 55, 429−441

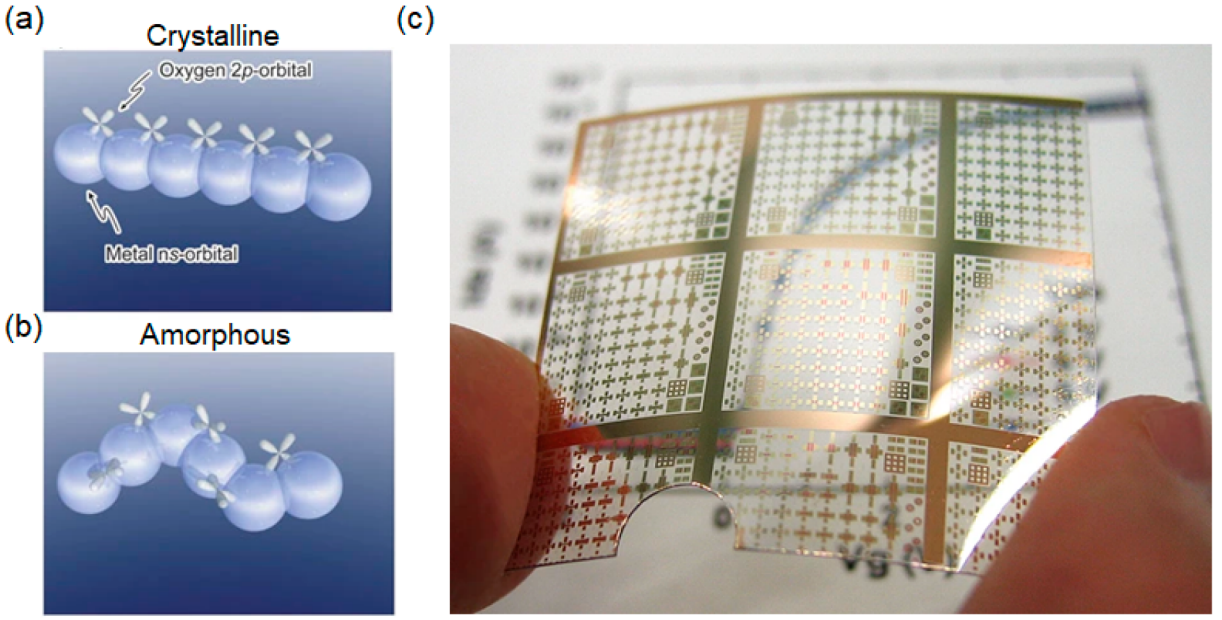

Figure 1. Schematic orbital illustrations of the carrier transport pathways in (a) crystalline and (b) amorphous MOs composed of post-transition-metal cations. Here the conduction band is composed of isotropic *s* orbitals (c) Amorphous IGZO TFTs fabricated on a plastic substrate. (a, b) Reproduced with permission from ref 8. Copyright 2004, Springer Nature. (c) Reproduced with permission from ref 18. Copyright 2018, Springer Nature.

and bias stress stability approaching the quality of industrial sputtered films.

- Wang, B.; Guo, P.; Zeng, L.; Yu, X.; Sil, A.; Huang, W.; Leonardi, M. J.; Zhang, X.; Wang, G.; Lu, S.; Chen, Z.; Bedzyk, M. J.; Schaller, R. D.; Marks, T. J.; Facchetti, A. Expeditious, scalable solution growth of metal oxide films by combustion blade coating for flexible electronics. *Proc. Natl. Acad. Sci. USA* **2019**, *116*, 9230−9238.[3] *Reports a highly efficient cofuel-assisted combustion process, which involves introducing both a fluorinated fuel and a preannealing step, that achieves ultrafast reaction times and metal−oxygen−metal lattice condensation within 10−60 s for representative MO semiconductors and an aluminum oxide dielectric.*
- Huang, W.; Chien, P. H.; McMillen, K.; Patel, S.; Tedesco, J.; Zeng, L.; Mukherjee, S.; Wang, B.; Chen, Y.; Wang, G.; Wang, Y.; Gao, Y.; Bedzyk, M. J.; DeLongchamp, D. M.; Hu, Y. Y.; Medvedeva, J. E.; Marks, T. J.; Facchetti, A. Experimental and theoretical evidence for hydrogen doping in polymer solution-processed indium gallium oxide. *Proc. Natl. Acad. Sci. USA* **2020**, *117*, 18231−18239.[4] *The performance of solution-processed IGO TFTs is greatly enhanced by poly(vinyl alcohol) doping, yielding a >70-fold increase in electron mobility. On achieving optimal H doping and conversion from six- to four-coordinate Ga, PVA addition suppresses deep trap defect localization.*

1. INTRODUCTION

Thin-film transistors (TFTs) are commonly utilized to amplify or to switch electronic signals, and they are key enabling components of modern electronic circuitry.[5,6] Owing to the high/stable electron mobilities, TFTs based on amorphous metal oxide (MO) semiconductors, such as indium−gallium−zinc oxide (IGZO), which bridge the performance gap between amorphous silicon (a-Si:H) and polysilicon TFTs, have achieved widespread commercialization when fabricated using conventional vapor-phase/photolithographic methodologies (Figure 1). However, MOs have additional appeal, such as solution processability from air-stable precursors (inks), mechanical properties compatible with emerging flexible/wearable electronics,[7−9] and processing temperatures as low as 150−300 °C, which are compatible with plastic substrates.[10−17] During the past decade, effective new approaches, such as photonic annealing, metal alkoxide precursors, CS, microwave-assisted annealing, high-pressure annealing, and polymer doping, have been developed and optimized for MO film growth.[19−22] Among them, CS and polymer doping are especially promising and do not require capital-intensive equipment or laborious precursor synthesis.[23]

2. COMBUSTION SYNTHESIS

2.1. Single Fuel Combustion

The first demonstration of thin (semi)conducting metal oxide film growth by a combustion process was reported for In_2O_3, a-IZO, and a-ZTO at processing temperatures of 200−400 °C. Indium nitrate, zinc nitrate, and tin chloride/ammonium nitrate were used as both the oxidizers and metal sources, while acetylacetone (AcAcH), or urea, was used as the fuel (Figure 2a).[1] Oxide formation via sol−gel processing is endothermic and requires significant external energy to decompose the precursor and form a densified M−O−M lattice, whereas CS is exothermic, thus does not require external energy once the reaction is ignited (Figure 2b). Thermal analyses of the dry CS precursors also indicate intense exotherms corresponding to ignition driving the reaction rapidly to completion (Figure 2c). For semiconductor applications in TFTs, the MO films should be very dense and with a thickness ranging between 10 and 100 nm thick, preferably ∼50 nm. This is challenging since CS generates so much heat and gaseous byproducts in a short time that decomposition of MO precursor films affording in one

https://doi.org/10.1021/acs.accounts.1c00671
Acc. Chem. Res. 2022, 55, 429−441

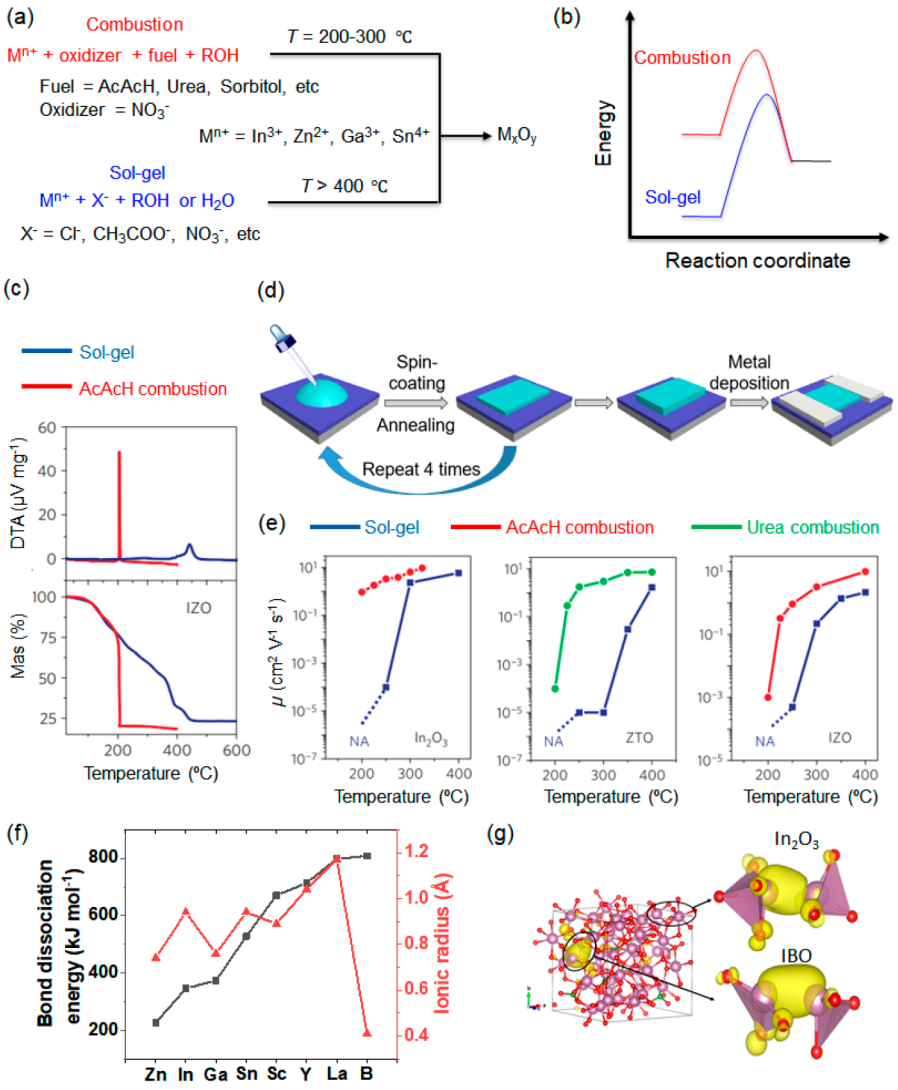

Figure 2. (a) Comparison of CS and conventional sol–gel MO film growth processes. (b) Energetics of CS vs conventional processes. (c) Thermal analyses of dried IZO sol–gel and combustion precursors. (d) Film and device fabrication procedures. (e) Carrier mobility μ versus annealing temperature for In_2O_3, ZTO, and IZO TFTs processed from different precursors. (f) Relevant M–O bond dissociation energies for MO_x compounds and ionic radii of the indicated metal ions. (g) DFT-AIMD computed charge density contours for the electron trap defect states in In_2O_3 and boron-doped In_2O_3 (IBO). (c, e) Reproduced with permission from ref 1. Copyright 2011, Springer Nature. (g) Reproduced with permission from ref 24. Copyright 2018, American Chemical Society.

step the desired MO thickness will create porosities.[2,7] Thus, to avoid these issues, we developed a procedure consisting of spin-coating/combusting ultrathin films from low MO precursor concentrations (~0.05 M) and achieving the desired semiconductor film thickness (>10 nm) via multiple spin-coating/combustion cycles (Figure 2d). Grazing incidence angle X-ray diffraction (GIAXRD) data from the resulting (multilayer) films processed at 200 °C indicate combustion precursor conversion to the desired In_2O_3 and ITO crystalline oxides at temperatures far lower than for sol–gel processing. Aluminum source–drain contacts were vapor-deposited on the MO films for TFT fabrication. As shown in Figure 2e, the combustion-derived MO TFTs exhibit much higher carrier mobility (μ), especially for those processed at temperatures <250 °C, than the sol–gel counterparts. Processing In_2O_3 and IZO films by combustion at 250 °C yields TFTs with μ of ~3.4 and ~0.9 $cm^2\ V^{-1}\ s^{-1}$ on SiO_2/Si substrates, respectively.

This approach was subsequently expanded to other MO semiconductors, including InXO (X = Sc, Y, La, B) and IXZO (X = Ga, Sc, Y, and La). These X elements exhibit much higher bond dissociation energies than In–O (Figure 2f)[25] and, thus, suppress In_2O_3 crystallization and act as oxygen "getters" to optimize the carrier concentration and TFT response durability under high gate voltages (bias-stress stability).[26] The results indicate that metal X cations with radii larger than that of In(III) can enhance amorphous character and enable high μ values at very low X concentrations (~5%).[27] Furthermore, increased cation size leads to broader tail-state trap distributions in the trap-limited conduction regime and greater potential barrier heights in the percolation regime.[5] We also investigated doping of In_2O_3 with boron (IBO), which was also found to frustrate In_2O_3 film crystallization as confirmed by X-ray diffraction data.[24] As shown in Figure 2g, ab initio molecular dynamics (AIMD) simulations with density-functional theory (DFT) calculations also show that the electron

https://doi.org/10.1021/acs.accounts.1c00671
Acc. Chem. Res. 2022, 55, 429–441

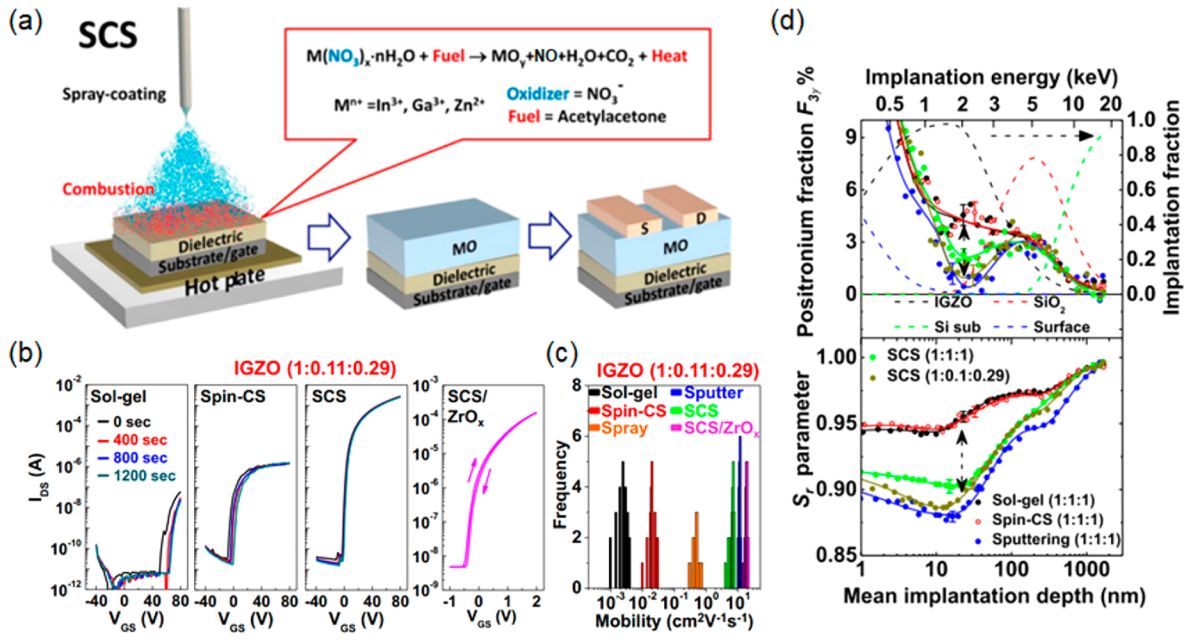

Figure 3. (a) Schematic of the spray-CS process used for growing MO films and the corresponding bottom-gate top-contact TFT structure. (b) Transfer characteristics and (c) Mobility distribution statistics for 50 nm-thick, single-layer IGZO TFTs fabricated by the indicated deposition methods. (d) PAS S_r and three-γ ortho-Ps annihilation ($F_{3\gamma}$) parameters for IGZO films as a function of the positron mean implantation depth. Reproduced with permission from ref 2. Copyright: The authors, some rights reserved; exclusive licensee *Proc. Natl Acad. Sci. USA*. Distributed under a Creative Commons Attribution License 4.0 (CC BY) https://creativecommons.org/licenses/by/4.0/.

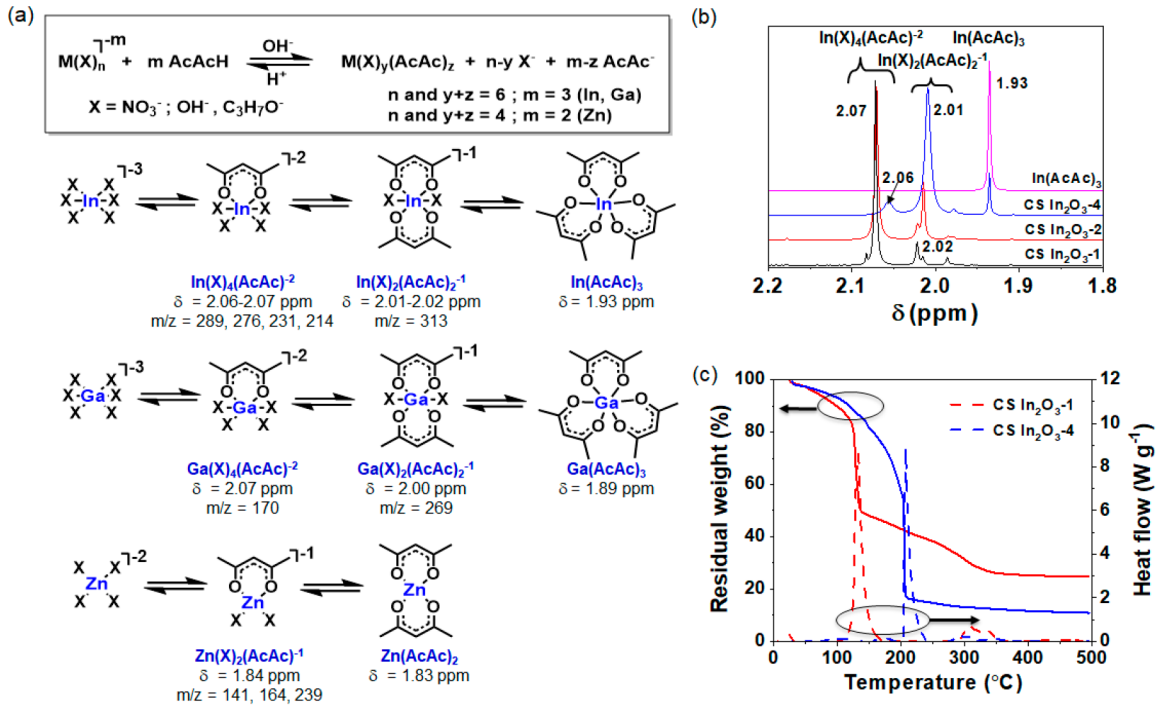

Figure 4. (a) Formation of metal acetylacetonate complexes in In_2O_3, Ga_2O_3, and ZnO precursor CS solutions, and the corresponding ^{1}H NMR chemical shifts and mass spectroscopic ion masses. (b) ^{1}H NMR spectra of CS In_2O_3 precursors and $In(AcAc)_3$ in DMSO-d_6, The molar ratio between metal (In) and AcAcH is 1:1, 1:2, and 1:4, respectively. (c) TGA and DSC curves of CS $In_2O_3{}^{-1}$ and $In_2O_3{}^{-4}$ precursors. Reproduced with permission from ref 31. Copyright 2019, Wiley-VCH Verlag GmbH & Co. KGaA, Weinheim.

density is localized between two undercoordinated In atoms, but that the coordination numbers of the two In atoms in B:$In_2O_{2.92}$ are far lower than those in $In_2O_{2.92}$ because of formation of deep/strongly localized defects. Optimized TFTs combining IBO channels with 6 at% B and a B:Al_2O_3 gate dielectric with 10 at% B exhibited a μ of ∼11 cm^2 V^{-1} s^{-1}, current on/off ratios >10^5, and superior bias stress stability.

To bypass multiple spin-coating/combustion coatings and enable continuous MO TFT fabrication, we invented a versatile new growth process combining continuous conformal

https://doi.org/10.1021/acs.accounts.1c00671
Acc. Chem. Res. 2022, 55, 429−441

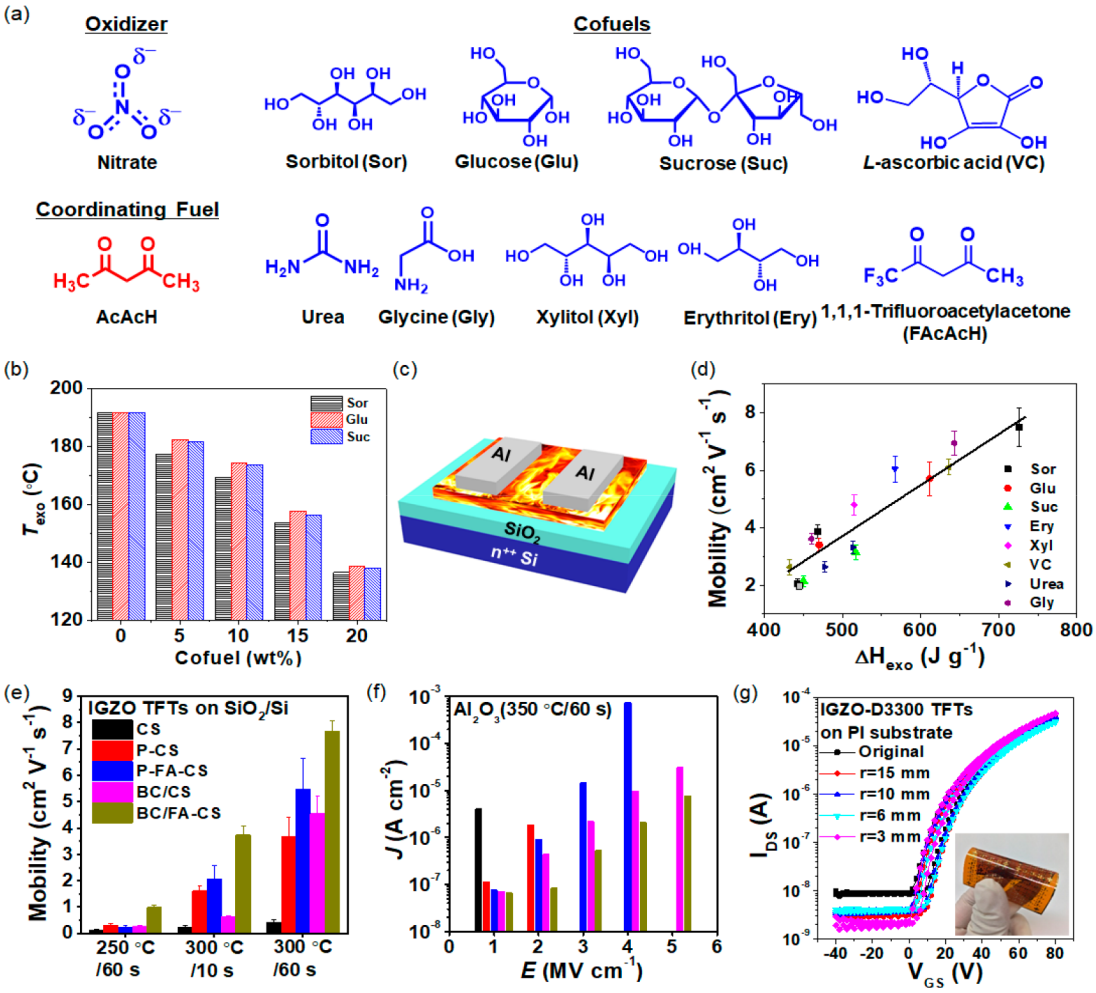

Figure 5. (a) Chemical structures of nitrate oxidizer, coordinating AcAcH fuel and cofuel. (b) Ignition temperature of FACS IGZO precursors with different cofuel types and contents. (c) Schematic of the IGZO TFT device structure. (d) Linear correlation between carrier mobility and enthalpy of combustion for different cofuels. (e) IGZO TFT mobilities on 300 nm SiO_2/Si with IGZO films processed by the indicated methods. (f) J–E curves of 350 °C/60 s Al_2O_3 dielectrics processed by the indicated methods. (g) Transfer curves of top-gate flexible IGZO TFTs as a function of bending radius. Reproduced with permission from ref 3. Copyright: The authors, some rights reserved; exclusive licensee *Proc. Natl Acad. Sci. USA*. Distributed under a Creative Commons Attribution License 4.0 (CC BY) https://creativecommons.org/licenses/by/4.0/.

spray-deposition with CS (SCS; Figure 3a).[2] Metal nitrates and AcAcH are used as oxidizer–fuel pair. Owing to the continuous drop-size delivery feature, SCS produces high-density, macroscopically continuous, conformal ~50 nm-thick IGZO films in short growth time (~30 min) versus 1.5 h for conventional spin-coating. Thus, 300 °C-processed SCS IGZO TFTs using 50 nm-thick IGZO films exhibit a maximum μ ~ 7.6 $cm^2\ V^{-1}\ s^{-1}$ and I_{on}: I_{off} ~ 10^8, which are ~10^3–10^4× greater than for the analogous sol–gel and spin-CS devices and approach the metric of commercial sputtered IGZO devices (Figure 3b and 3c). As shown in Figure 3d, positron annihilation spectroscopy (PAS), a technique to correlate positron lifetime with film porosity, indicates that SCS IGZO (1: 0.1: 0.29) and sputtered IGZO films are the least porous with the subnanometer porosities estimated at ~6%, followed by SCS IGZO with a porosity of ~10%. The sol–gel and spin–CS films have significantly higher porosity of >15%. In subsequent work, optically transparent all-SCS processed all-oxide TFTs were fabricated, integrating high-quality ZrO_2 or Al_2O_3 gate dielectrics, an IGZO semiconductor channel, and ITO conducting electrodes in the same platform.[28] These all-oxide transparent IGZO TFT arrays achieve maximum mobilities of ~8 $cm^2\ V^{-1}\ s^{-1}$ at operating voltages <3 V.

In principle, the combustion growth process can be well-described by the Arrhenius formalism and reaction kinetics.[29] MO film quality, which correlates with device performance, strongly depends on the precursor composition (related to activation energy), annealing temperature, and time. Thus, understanding those factors governing combustion precursor (ink) efficacy is critically important. For combustion precursors $M(NO_3)_x$, AcAcH, NH_4OH, and 2-methoxyethanol, the interaction between $AcAc^-$, M^{x+}, and other species ($C_3H_7O_2$, OH^-, and NO_3^-) depends on the metal–AcAc stability constant (expressed by the product of the concentration of products divided by the product of the concentrations of the reactants),[30] the M:AcAcH ratio, and the pH (Figure 4a).[31] These variables can be assessed by ^{1}H NMR (Figure 4b) and electrospray ionization mass spectrometry (ESI-MS). Thus, different metal–AcAc coordinations are expected to affect the thermal behavior during combustion process. For instance, from the DSC/TGA data (Figure 4c), the CS In_2O_3 precursor ignition temperatures decrease substantially from ~206 to 133 °C as the In:AcAcH molar

https://doi.org/10.1021/acs.accounts.1c00671
Acc. Chem. Res. 2022, 55, 429–441

ratio falls from 1:4 to 1:1. However, more heat is evolved on moving from the $In(AcAc)_3$ to undercoordinated AcAc species. Specifically, the ΔH_{exo}/RW (RW = residual weight) increases from ~460 J g^{-1}/13.2% to ~737 J g^{-1}/31.5% as the In:AcAcH molar ratio is increased from 1:1 to 1:4. Thus, not only how rapidly the combustion occurs but also how efficiently it thermolyzes the precursors, reflects a balance between heat evolved and chemical species present, and is crucial for optimizing the resulting oxide TFT performance.[31]

2.3. Dual Fuel Combustion

Unlike bulk combustion processes, the loss of reactants because of the high surface-to-volume ratio in thin film combustion can result in inefficient precursor to MO film conversion. These results raise the intriguing question as to whether more effective/exothermic fuels than AcAcH can be devised.[32] Carbohydrates (sorbitol, sucrose, and glucose) are remarkably effective propellants in "rocket candy",[33] and thus, we investigated them for the CS of MO thin films (Figure 5a).[7,34] Interestingly, when used as the sole fuel with metal nitrates, combustion does not occur. However, when AcAcH is used as a coordinating fuel and the sugars as cofuels, the combustion is very efficient. This reaction is termed fuel-assisted-CS (FA-CS) and is found to significantly lower the ignition threshold temperature (T_{exo}) (Figure 5b) and, for optimal stoichiometries, enhance the reaction enthalpy. Specifically, the FA-CS reduces the T_{exo} of the dried IGZO precursors from 165−210 °C to 112−171 °C (depending on the M^+ and AcAcH molar ratio) and increases the combustion enthalpy from ~200 to ~450 kJ mol^{-1}. The microstructural changes within the amorphous MO films were analyzed by In EXAFS to extract the In^{3+} coordination numbers (N_i) and bond lengths (R_i) for the ligand atoms of interest. The FA-CS IGZO film with an optimized sorbitol content exhibits an N_i of 5.39, higher than that (5.12) of, the conventional CS film. The extracted CS and FA-CS IGZO film R_i values are relatively constant at ~2.16 Å for the In−O shell and ~3.35 Å for the In-M shell. Regarding the IGZO TFT performance in a bottom-gate top-contact architecture (Figure 5c), μ increases from ~2.0 to 3.2−7.5 cm^2 V^{-1} s^{-1}, while the bias stress instability threshold voltage shift, ΔV_T, falls from ~14 to ~1.7 V. More recently FACS was extended to the cofuels, urea, glycine, L-ascorbic acid, erythritol, and xylitol. Among them, the L-ascorbic acid for the FACS IGZO lowers the T_{exo} by ~65 °C vs the conventional CS process. A combination of ^1H NMR, ESI-MS, and GIXRD analysis indicates that these cofuels influence the metal cation coordination of the primary AcAcH fuel in the precursors, thus altering the combustion pathway and affording enhanced TFT performance. Clear correlations between precursor combustion enthalpy, a-MO densification, and electron mobility were established (Figure 5d).

To expedite the MO film/TFT combustion processing times even further, we recently developed a new approach using a volatile cofuel (1,1,1-trifluoro-2,4-pentanedione, FAcAcH) in the precursor solutions and employing a brief low-temperature prebaking step (120 °C/60 s) before combustion, called P-FA-CS.[3,35,36] Removing most solvent from the precursor film prior to the combustion onset and enhancing the combustion heat dramatically shortens the postcombustion annealing times from ~20 min to as little as 10−60 s for each MO layer. The scope of this approach was demonstrated for In_2O_3, IZO, and IGZO semiconductors and an Al_2O_3 dielectric. To better understand the origin of this high-efficiency combustion process, IGZO films processed by different procedures were characterized by X-ray reflectivity (XRR), to assess the film thickness and average electron density (ρ_{avg}). The conventional CS IGZO film processed at 300 °C/20 min yields ρ_{avg} = 1.50 e $Å^{-3}$, lower than that of the corresponding 300 °C/60 s-annealed P-FA-CS IGZO films (1.53 e $Å^{-3}$). Interestingly, the 300 °C/60 s-annealed P-FA-CS IGZO films have a thickness (10.5 nm) that is slightly less than that (10.7 nm) of the conventional CS IGZO films 300 °C/20 min annealing, indicating that prebaking and FA-CS significantly enhances film densification. Finally, we demonstrated that FA-CS is compatible not only with spin-coating but also with blade-coating (BC), which is effective for the expeditious wafer-scale fabrication of IGZO TFTs. As shown in Figure 5e and 5f, the BC-derived IGZO TFTs have the highest electron mobility and bias stability, and the BC-derived Al_2O_3 dielectric has the highest breakdown field. The 300 °C/60 s-derived IGZO TFTs with a top-gated polymer dielectric on flexible polyimide substrates provides high mechanical flexibility to a 3 mm bending radius (Figure 5g) and good TFT bending stability, which is measured after bending at a radius of 6 mm repeatedly for up to 1000 cycles.

3. POLYMER DOPING

3.1. PEI Doping

Another effective semiconducting MO solution processing strategy developed by this Laboratory is polymer doping of MOs which, when research was initiated, was completely uncharted territory. It not only modifies film charge carrier concentrations and crystallinity, but also holds the potential to yield enhanced MO performance and more mechanically flexible devices. Note, because of the incompatibility of the combustion precursors with those used in current polymer doping, all the polymer doping of metal oxides described below is carried out using sol−gel chemistries.

In the first study, it was demonstrated that adding poly(4-vinylphenol) (PVP) to $In(NO_3)_3$ precursor solutions greatly reduces In_2O_3 film crystallinity but permits a sufficient density of interconnected InO_x polyhedra for efficient charge transport (Figure 6a).[37] We next investigated several compositions where the PVP weight content in the precursor was varied from 0% to 20%, and TFTs were fabricated on SiO_2/Si substrates with Al source/drain contacts. Figure 6b and 6c shows that the transfer curve of a neat In_2O_3 TFT exhibits a high off-current and low on/off current ratio (I_{on}/I_{off}) of 10^4, while the In_2O_3:5 wt % PVP TFT exhibits a desirable low off-current (10^{-10} A) and high I_{on}/I_{off} of 10^7. Regarding μ, it falls from ~3.2 cm^2 V^{-1} s^{-1} for neat In_2O_3 (0% PVP) TFTs to ~2.1 to ~0.16 cm^2 V^{-1} s^{-1} for the In_2O_3:5 wt % PVP and In_2O_3:20 wt % PVP blend TFTs, respectively (Figure 6d).

These intriguing results prompted us to consider whether other functional polymers, especially electron-rich polymers, could be incorporated into inorganic oxides and what the effect on MO electronic properties might be. Thus, PEI (Figure 7a), a commercially available polymer containing one of the highest amino group densities among all known polymers, was investigated first.[38−40] GIXRD reveals that PEI incorporation in In_2O_3 can also impede crystallization and promotes amorphization. As seen from the cross-sectional transmission electron microscopy (CS-TEM) of Figure 7b and 7c, the neat In_2O_3 film is relatively uniform in the vertical direction and features a mixture of lighter and darker regions. Higher

https://doi.org/10.1021/acs.accounts.1c00671
Acc. Chem. Res. 2022, 55, 429−441

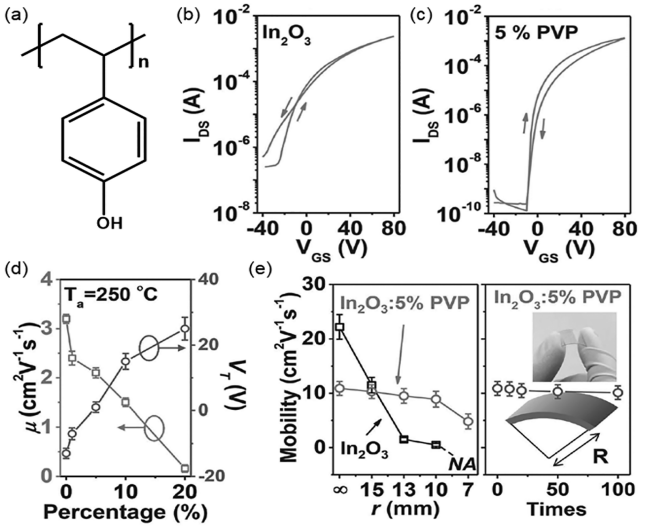

Figure 6. (a) Chemical structure of PVP. Transfer curves of (b) In_2O_3 and (c) In_2O_3:5 wt % PVP TFTs processed at 250 °C. (d) TFT mobility and threshold voltage for In_2O_3:polymer films having different PVP concentrations, processed at 250 °C. (e) Dependence of TFT mobilities on bending radius of both neat In_2O_3 TFTs and all-amorphous In_2O_3:5 wt % PVP TFTs, and mobilities on all-amorphous TFT bending cycles at a radius of 10 μm. Reproduced with permission from ref 37. Copyright 2015, Wiley-VCH Verlag GmbH & Co. KGaA, Weinheim.

magnification TEM indicates that the In_2O_3 film is polycrystalline. In contrast, PEI doping of the In_2O_3 films strongly frustrates crystallization and the TEM image of the In_2O_3:1.5 wt % PEI film clearly shows the formation of well-defined 3-layer structures. FTIR spectroscopy (Figure 7d) reveals N−H bending/stretching modes, meaning that amine/ammonium groups remain in the blend. The transport characteristics of the In_2O_3:x wt % PEI TFTs reveal that PEI doping has a profound influence on TFT performance (Figure 7e).

Representative transfer plots indicate that incorporating >1 wt % PEI leads to lower I_{off} (from ~10^{-7} A to ~10^{-11} A). Interestingly, I_{on} first increases from 1.54×10^{-3} (0.0% PEI) to 2.96×10^{-3} A (1% PEI) and then falls as more PEI is incorporated. The measured mobility first increases, reaching a peak (μ_{peak}), and then falls. Thus, μ first increases from ~4.2 to a μ_{peak} of ~8.3 cm^2 V^{-1} s^{-1} when PEI increases from 0.0 wt % to 1.0−1.5 wt %, then falls to ~4 cm^2 V^{-1} s^{-1} at PEI concentrations of 2.0−2.5 wt %, and then falls further to ≤1 cm^2 V^{-1} s^{-1} at >6 wt % PEI concentration (Figure 7f). Simultaneously, V_{th} (the TFT threshold voltage) monotonously shifts to more positive values as the PEI concentration rises, reaching an optimal value of ~0.0 V for PEI levels of 1.0−1.5 wt %. A two-layer structure TFT was also fabricated with PEI coated on top of a prefabricated neat In_2O_3 device to assess the PEI electron donating capability (Figure 7g). After coating, the I_D is always larger than 10^{-3} A at various gate voltages, verifying the strong electron doping capacity of PEI for In_2O_3. In contrast, devices with PEI alone show a current lower than 10^{-9} A, corroborating the insulating nature of the neat polymer. In subsequent work, TFTs with other metal oxide:PEI blends (IZO, In:Zn = 70:30; IGO, In:Ga = 70:30; IGZO, In:Ga:Zn = 72.5:7.5:20 mol ratios) were fabricated to verify the PEI doping generality (Figure 7h). Specifically, when incorporating PEI into IZO (In:Zn = 70:30) and IGO (In:Ga:Zn = 72.5:7.5:20), the optimal PEI concentrations to achieve μ_{peak} shifts to lower PEI contents, from 1.0 wt % in In_2O_3 and IGO to 0.5 wt % in IZO and IGZO. Figure 7i shows the μ_{peak} for several MO:PEI blends, along with the mobility of the corresponding undoped MO matrices. From this composition−mobility plot, it can be seen that the oxide matrix mobilities fall as the Ga and/or Zn content rises. Similar trends are also found for the peak mobility of the MO:x wt % PEI TFTs with optimal PEI contents. Furthermore, it was found that PEI capacity to increase mobility is more pronounced when the neat MO film is polycrystalline and for compositions rich in Ga and/or Zn.

Ultraviolet photoelectron spectroscopy (UPS) measurements were next carried out on these MO systems and revealed that PEI doping of the MO effectively lowers the WF, meaning that PEI transfers electrons to the oxide matrix, and the transfer process is composition-dependent. For example, the WF of the IGO (70:30, 300 °C) film shifts monotonically from 4.22 (0.0 wt % PEI) to 3.97 eV (6 wt % PEI). Finally, to underscore the relationship between PEI electron doping capacity, the appearance of a mobility peak, achieving optimal PEI doping level, and the MO film electronic structure, the optimal PEI content yielding the maximum mobility is plotted as a function of the WF for the various neat metal oxide matrices in Figure 7j. This result agrees with a smooth transition upon PEI addition from a polycrystalline to amorphous phase, which reduces gain boundary scattering and suggests that for these low WF/polycrystalline compositions, PEI is more effective in enhancing mobility via promoting amorphization, than by optimal trap prefilling with PEI-derived electrons.

Based on this detailed understanding of PEI electron doping effects in these MO systems, it can be seen that the Fermi level (E_F) of In_2O_3 is tunable over the range of 3.62−4.0 eV with differing PEI contents (Figure 8a), making it possible to construct In_2O_3 homojunctions.[41] In related work, four different transistors (TFT1−TFT4) with bilayer In_2O_3 with/without 1 wt % PEI (see Figure 8b) were fabricated and characterized. TFTs with 1 wt % PEI doped In_2O_3 layers invariably show higher I_{on} metrics than those with neat In_2O_3 (see Figure 8c). Especially for TFT-4, the highest I_{on} of 3.30×10^{-3} A is obtained, which is more than 3× higher than the 9.66×10^{-4} A of TFT-1 (neat In_2O_3).

As shown in Figure 8d, TFT-1 having two identical pristine In_2O_3 layers exhibits an electron mobility of ~4.16 cm^2 V^{-1} s^{-1}, while incorporating PEI in both or either top/bottom In_2O_3 layers enhances the mobility to ~6.0 cm^2 V^{-1} s^{-1} in TFT-2, ~6.3 cm^2 V^{-1} s^{-1} in TFT-3, and ~10.1 cm^2 V^{-1} s^{-1} in TFT-4. The large mobility enhancement in TFT-4 can be ascribed to the heterojunction forming a two-dimensional electron gas (2DEG) near the In_2O_3:PEI/In_2O_3 interface because of E_F alignment. Variable-temperature I−V measurements of TFT-4 (1.0 and 4.0 wt % PEI) and TFT-1 were carried out to further probe the electron transport mechanism in these homojunction devices. Figure 8e shows Arrhenius plots of saturation mobility over 50−290 K for TFT-1 and TFT-4. Overall, the mobility of TFT-1 falls more rapidly than that of TFT-4 with falling temperature, and the TFT-1 device clearly exhibits thermally activated behavior, typical of trap-limited conduction in MO TFTs.[42] In marked contrast, TFT-4 (1 or 4 wt % PEI) shows far weaker temperature dependence, with μ_e saturating at ~4 cm^2 V^{-1} s^{-1} at low temperatures, consistent with percolation conduction.[43] Thus, TFT-4 charge conduction occurs via formation of a 2DEG at the intrinsic and

https://doi.org/10.1021/acs.accounts.1c00671
Acc. Chem. Res. 2022, 55, 429−441

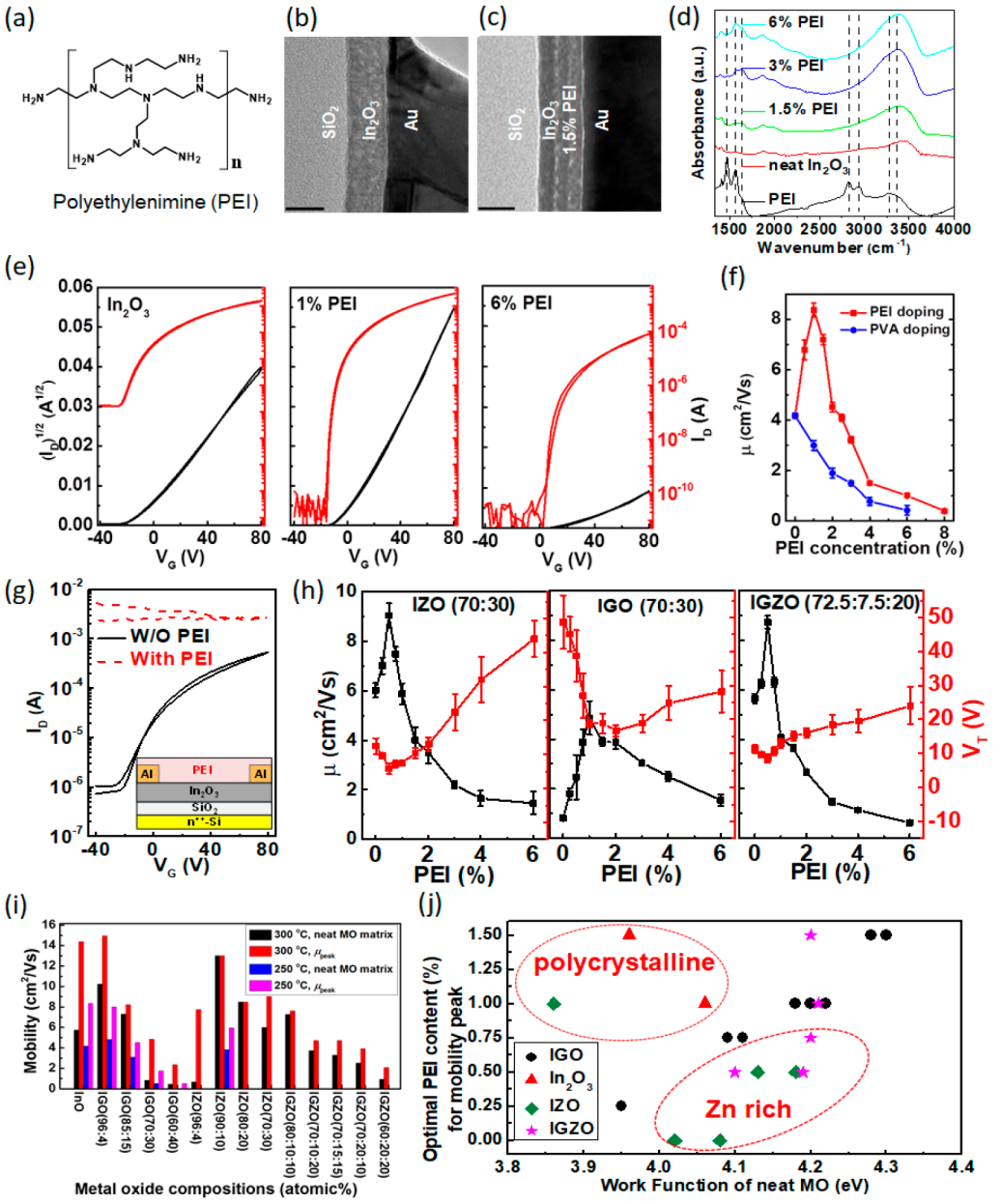

Figure 7. (a) Chemical structure of PEI. Cross-sectional TEM images of (b) neat In_2O_3 film and (c) In_2O_3:1.5 wt % PEI film. The scale bars are 10 nm. (d) FT-IR spectra of In_2O_3:*x*% PEI blend films with differing PEI contents. (e) Representative transfer plots for the indicated In_2O_3:*x*% PEI TFTs; V_D = +80 V. (f) TFT electron mobility for In_2O_3:*x*% PEI devices as a function of the polymer concentration. (g) Transfer plots of In_2O_3 TFTs with/without PEI coated on the transistor with ∼9 nm In_2O_3 layer and PEI coated on the electrical contacts; V_D = +80 V. (h) TFT mobility and threshold voltage for IZO:*x* wt % PEI, IGO:*x* wt % PEI, and IGZO:*x* wt % PEI, as a function of the polymer content. T_{ann} = 300 °C. (i) Mobilities of neat MO TFTs and peak mobilities of the corresponding PEI-doped MO TFTs with optimal PEI content. (j) Optimal PEI content (wt %) yielding maximum mobility with respect to the WF (work function) of the indicated neat MO matrices. (d−g) Reproduced with permission from ref 38. Copyright 2016, Wiley-VCH Verlag GmbH & Co. KGaA, Weinheim. (b−c, h−j) Reproduced with permission from ref 39. Copyright 2018, American Chemical Society.

doped In_2O_3 layer interface. The physical distance between this plane of high carrier density and the gate dielectric surface is expected to suppress both long-range Coulomb scattering by trapped charges and short-range scattering from dielectric surface topological imperfections and chemical defects.

Recently, correlations between polymer structure and charge transport in solution-processed In_2O_3:polymer blend TFTs were investigated using four amino-polymers with varied atomic amine nitrogen content (N% = 0.0−12.6%). These amino-polymers influence the In_2O_3 TFT mobilities via a delicate interplay of electron transfer/doping, charge generation/trap-filling, and film morphological/microstructural variations, which depend on the polymer architecture, thermal stability, and N%, as well as the polymer content of the In_2O_3 precursor and the carbon residue content in the In_2O_3. Thus, increasing the N% from 0.0% in the control PVP to 12.6% in PEI increases the polymer electron doping capacity, the polymer content of the blend formulation, and the blend TFT mobility. Optimal polymer incorporation invariably enhances

https://doi.org/10.1021/acs.accounts.1c00671
Acc. Chem. Res. 2022, 55, 429−441

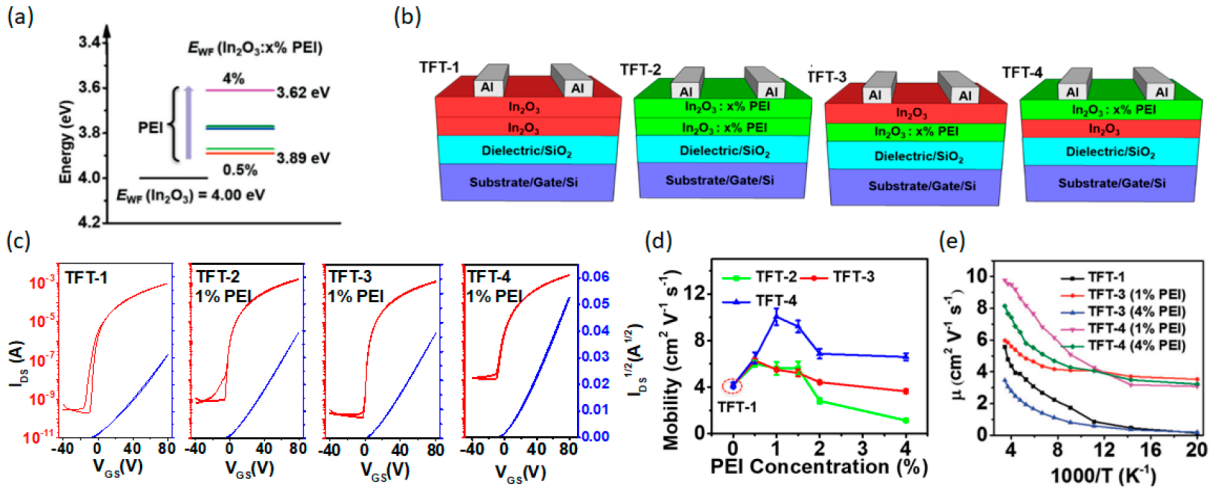

Figure 8. (a) Schematic energy band diagram illustrating the shift of E_{WF}. (b) Four different TFT structures used in this study and (c) Representative transfer characteristics. (d) Mobility versus PEI content (wt %) for the indicated devices. (e) Plot of the μ of TFT-1, TFT-3, and TFT-4 (1.0 and 4.0 wt % PEI) transistors as a function of inverse temperature measured between 290 and 50 K. Reproduced with permission from ref 41. Copyright 2019, Wiley-VCH Verlag GmbH & Co. KGaA, Weinheim.

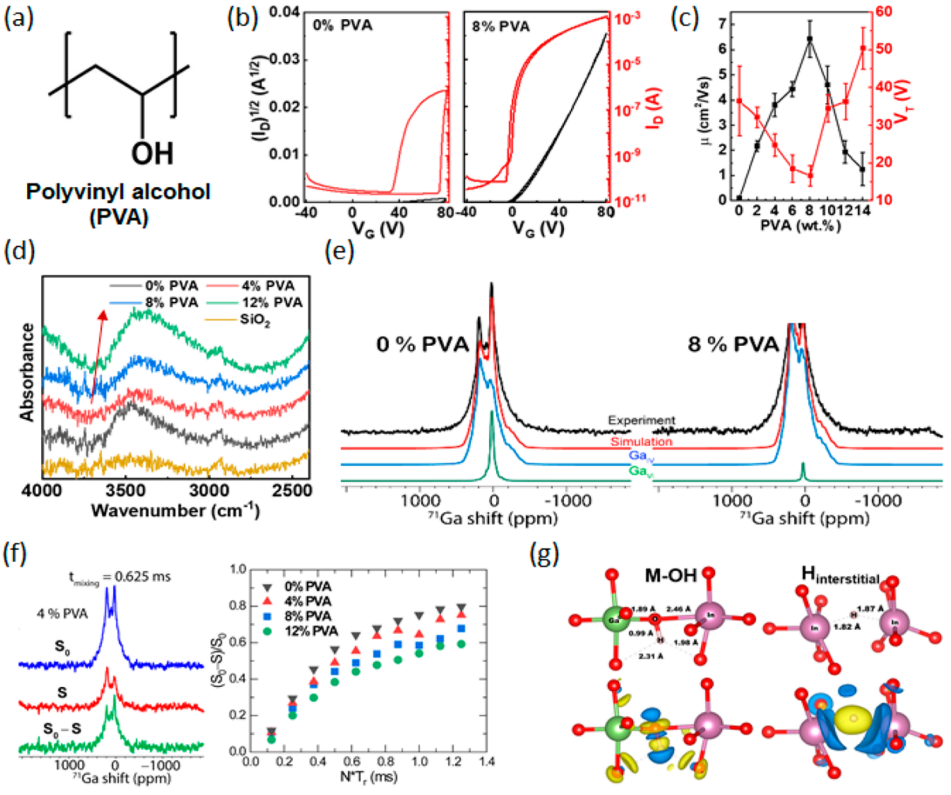

Figure 9. (a) Chemical structure of PVA. Characterizations of IGO:PVA TFTs as a function of PVA content: (b) representative transfer curves (V_{DS} = +80 V) and (c) μ and V_T of IGO:PVA TFTs. (d) ATR FT-IR of the IGO:PVA films. (e) Representative ^{71}Ga MAS NMR spectra of IGO:PVA powders with and without 8% PVA. (f) ^{71}Ga{^{1}H} REDOR NMR for determining Ga−H distance. An example of the ^{71}Ga NMR spectra without dephasing (S_0) and with dephasing (S), along with the difference ($\Delta S = S_0 - S$) after a mixing time of 0.625 ms, and the ^{71}Ga{^{1}H} REDOR curves of IGO:PVA with varied PVA content as a function of mixing times. (g) Calculated most energetically stable OH bond, and H interstitial in $In_{32}Ga_{22}O_{80}H_1$. In each case, the calculated Bader charge transfer is shown as positive (yellow) and negative (blue) charge density differences. Reproduced with permission from ref 4. Copyright: The authors, some rights reserved; exclusive licensee *Proc. Natl. Acad. Sci. USA*. Distributed under a Creative Commons Attribution License 4.0 (CC BY) https://creativecommons.org/licenses/by/4.0/.

charge transport by as much as ∼2×, leading to a μ_{peak} of ∼8.5 cm^2 V^{-1} s^{-1} on Si/SiO$_2$ substrates.

3.2. PVA Doping

When polymer doping of In_2O_3 was first investigated as a control experiment using poly(vinyl alcohol) (PVA), the expected result was that this polymer, devoid of amine

https://doi.org/10.1021/acs.accounts.1c00671
Acc. Chem. Res. 2022, 55, 429−441

nitrogens, was incapable of donating electrons, and In_2O_3 TFT performance was expected to be poor (Figure 7f). However, it was discovered that adding PVA (Figure 9a) to IGO (In:Ga = 6:4 mol ratio) precursor solutions dramatically enhances TFT charge transport.[4] Thus, IGO:PVA TFTs exhibit more than 1000× greater I_{on} enhancement, and >70-fold increase in electron mobility for films processed at 300 °C, leading to a high μ of ∼7.9 versus ∼ 0.1 $cm^2\ V^{-1}\ s^{-1}$ for the pristine IGO device, which is among the highest mobilities ever achieved for IGO TFTs with such a high Ga content at such a low processing temperature (Figure 9b and 9c).

Using a battery of characterization techniques, we explained this result as a H-doping effect. Thus, the OH content in IGO:PVA film was quantified by ATR FT-IR spectroscopy (Figure 9d). Neat IGO films exhibit relatively strong O−H stretching modes at 3200−3600 cm^{-1}, centered near ∼3470 cm^{-1}, while PVA addition to 4 and 8 wt % IGO:PVA weakens the O−H mode, with a gradual shift toward 3450 cm^{-1} (4 wt %) and 3410 cm^{-1} (8 wt %), consistent with enhanced O−H covalency or O−H···O bond formation.[44] Resonant soft X-ray scattering (R−SoXS) shows no obvious change in profile shape at off-resonant or near-resonant energies, suggesting that PVA significantly thermolyzes during film fabrication and does not introduce phase separation in the resulting IGO films. Furthermore, ^{71}Ga MAS NMR reveals that the majority (>85%) of Ga sites are four-coordinate (Ga_{IV}). As the PVA content is increased, the six-coordinate Ga (Ga_{VI}) fraction gradually falls from 13.8% (pristine IGO) to 1.3% (8 wt % PVA) (Figure 9e). The large nuclear quadrupolar coupling constant, C_Q, in all the four samples indicates that Ga, especially Ga_{IV}, is in a severely distorted low-symmetry local environment. Figure 9f shows REDOR NMR experiments on IGO:PVA powders. It was found that the build-up rate of the ^{71}Ga signal, $\Delta S/S_0$, decreases with higher PVA content. As the PVA content increases, the −OH in IGO:PVA powders leads to slower ^{71}Ga dephasing by ^{1}H, and $\Delta S/S_0$ decreases from 0.56 (no PVA) to 0.49 (4 wt % PVA), to 0.44 (8 wt % PVA), and to 0.38 (12 wt % PVA) at a 0.5 ms dipolar decoupling time (N^*T_r). The slower $\Delta S/S_0$ build-up in the IGO:PVA powders indicates ineffective dephasing of ^{71}Ga magnetization. Second moment (M2) REDOR data analysis within the $\Delta S/S_0 < 0.3$ range yields average H−Ga distances, which increase from 3.23 ± 0.33 (no PVA) to 3.36 ± 0.34 Å (8 wt % PVA).

On the basis of these experimental results, DFT analysis and AIMD liquid-quench simulations were performed to further elucidate the H-doping effects in amorphous IGO. It is found that the presence of H reduces the localization of deep electron traps (Figure 9g). Before H doping, the trapped electron is localized between two undercoordinated under-shared In ions. Upon OH^- formation, the trapped charge density is found at two separate locations. Integration of the charge distribution reveals that each area with localized charge contains only ∼0.5 $\bar{e}$ suggesting an equal probability of finding the electron in either of the two locations. Indeed, the localization of the deep defect decreases by almost one-half as compared to the H-free material. These results demonstrate that Ga in oxide semiconductors acts not only as an oxygen getter, but also can readily change coordination number from 6 to 4, particularly in the presence of PVA. This effectively increased low-coordinated O content will attract H and enhance the electrical properties. Moreover, the H in such IGO:PVA films decreases the local distortion of all neighboring metal polyhedra, increasing free carrier transport by providing more uniform conduction charge density, and also suppress the localization of deep electron traps.

4. CONCLUSIONS

The CS and polymer doping of MO films for TFT applications were discussed in this Account. Particular attention is paid to precursor/film chemistry and its correlation with device performance. The metal nitrates and acetylacetones are the most efficient oxidizer-fuel pairs, while the addition of cofuels greatly lowers the ignition temperature, enhancing the combustion heat and device performance. Regarding polymer doping, PEI and PVA, rich in amine/hydroxyl groups, provide efficient electron and hydrogen doping, respectively. Comprehensive and integrated characterization techniques including GIXRD, XRR, EXAFS, R-SoXS, TEM, NMR spectroscopy, mass spectrometry, FT-IR spectroscopy, UPS, thermal analysis, and theoretical analyses (DFT, AIMD) are important in understanding the origin of these remarkable phenomenon, as well as the microstructure and electronic structure of these MO precursors and films.

The broad generality of thin-film combustion and polymer doping methodologies are demonstrated for several MO materials, and processing temperatures from 200 to 300 °C have been utilized to achieve morphologically and electrically high-quality MO films. More promising, recent reports have shown that CS annealing times can be greatly shortened from ∼1.5 h to <5 min, making it truly compatible with large-scale roll-to-roll fabrication. Nevertheless, processing temperatures near 250 °C are still required to achieve high-performance ternary or quaternary MO films containing strong oxygen getters, such as Ga^{3+}, Sc^{3+}, Y^{3+}, and La^{3+}. The combination of CS/polymer doping with other low-temperature methods (e.g., photonic annealing) may further reduce the annealing temperatures, making them compatible with engineering/common plastic substrates having glass transition temperatures of 100−150 °C. Furthermore, exploring new applications of these low-temperature processed, high-performance MO films is critically important beyond the pioneering demonstrations of n-type MO TFTs, memories, solar cells, and batteries.[23,45−47] Lastly, engineering MOs into interwoven MO fiber electronics (fibertronics) illustrates a new concept to transform fragile MOs into modalities suitable for stretchable and wearable electronics.[48]

The most successful a-MO semiconductor is IGZO, which is used in driving TFTs for advanced flat-panel displays. Although IGZO TFTs fabricated by capital-intensive sputtering method is a mature industrial process, the pursuit for cost-effective, large-area, roll-to-roll compatible solution-processed (e.g., inkjet-printed) TFTs continues. However, challenges to achieving this goal include ink stability, film uniformity, device performance, batch-to-batch consistency, and large process windows for implementation in production lines. The CS and polymer doping discussed here clearly enhance device performance and shorten annealing time on a laboratory scale. Close collaboration with industry is necessary for future pilot tests and performance realization at scale.

AUTHOR INFORMATION

Corresponding Authors

Tobin J. Marks − *Department of Chemistry and the Materials Research Center, Northwestern University, Evanston, Illinois 60208, United States; Department of Materials Science and*

https://doi.org/10.1021/acs.accounts.1c00671
Acc. Chem. Res. 2022, 55, 429−441

Engineering, and the Materials Research Center, Northwestern University, Evanston, Illinois 60208, United States; orcid.org/0000-0001-8771-0141; Email: t-marks@northwestern.edu

Antonio Facchetti − *Department of Chemistry and the Materials Research Center, Northwestern University, Evanston, Illinois 60208, United States; Flexterra Corporation, Skokie, Illinois 60077, United States;* orcid.org/0000-0002-8175-7958; Email: a-facchetti@northwestern.edu

Authors

Binghao Wang − *Joint International Research Laboratory of Information Display and Visualization, School of Electronic Science and Engineering, Southeast University, Nanjing, Jiangsu 210096, China; Department of Chemistry and the Materials Research Center, Northwestern University, Evanston, Illinois 60208, United States;* orcid.org/0000-0002-9631-6901

Wei Huang − *Department of Chemistry and the Materials Research Center, Northwestern University, Evanston, Illinois 60208, United States; School of Automation Engineering, University of Electronic Science and Technology of China (UESTC), Chengdu, Sichuan 611731, China;* orcid.org/0000-0002-0973-8015

Michael J. Bedzyk − *Applied Physics Program, Department of Materials Science and Engineering and Department of Materials Science and Engineering, and the Materials Research Center, Northwestern University, Evanston, Illinois 60208, United States;* orcid.org/0000-0002-1026-4558

Vinayak P. Dravid − *Department of Materials Science and Engineering, and the Materials Research Center, Northwestern University, Evanston, Illinois 60208, United States;* orcid.org/0000-0002-6007-3063

Yan-Yan Hu − *Department of Chemistry and Biochemistry, Florida State University, Tallahassee, Florida 32306, United States;* orcid.org/0000-0003-0677-5897

Complete contact information is available at: https://pubs.acs.org/10.1021/acs.accounts.1c00671

Author Contributions

†B.W. and W.H. contributed equally.

Notes

The authors declare no competing financial interest.

Biographies

Binghao Wang is a Professor at Southeast University, China. Prior to this, he was a Project Researcher at The University of Tokyo and a Joint-PhD student/Postdoctoral Researcher at Northwestern University. He obtained his B.E., M.S., and PhD from Soochow University.

Wei Huang is a Professor at University of Electronic Science and Technology of China. Prior to this, he was a Joint-PhD student, Postdoctoral Researcher, and Research Assistant Professor at Northwestern University.

Michael J. Bedzyk is a Northwestern University Professor of Materials Science & Engineering and Physics & Astronomy. He is a Fellow of the American Physical Society and the American Association for the Advancement of Science, and received the Warren Award for Diffraction Physics. His PhD is in Physics from the State University of New York at Albany.

Vinayak P. Dravid is Abraham Harris Professor of Materials Science and Engineering at Northwestern University and the founding Director of NU Atomic and Nanoscale Characterization Experimental (NUANCE) Center. He received his B.Tech. from IIT Bombay and PhD from Lehigh University.

Yan-Yan Hu is an Associate Professor at Florida State University. She received her B.S. degree from Tsinghua University and PhD from Iowa State University. Her research interest is the development of solid-state NMR/MRI techniques and applications of these techniques to material characterizations.

Tobin J. Marks is the Vladimir N. Ipatieff Professor of Chemistry and Professor of Materials Science and Engineering at Northwestern University. He received his B.S. degree from the University of Maryland and PhD from MIT. He is a fellow of the American Academy of Arts and Sciences, the U.S. National Academy of Sciences, the National Academy of Engineering, and the National Academy of Inventors.

Antonio Facchetti obtained his Laurea and PhD from the University of Milan. He, then, carried out postdoctoral research at the University of California−Berkeley and Northwestern University. In 2002, he joined Northwestern University, where he is currently an Adjunct Professor. He is a cofounder and, currently, the CTO of Flexterra, Inc.

■ ACKNOWLEDGMENTS

We thank AFOSR (FA9550-18-1-0320), the Northwestern University MRSEC (NSF DMR-1720139), and Flexterra, Inc., for support of this research. B.W. thanks the research startup fund of Southeast University (4306002172). We also thank our numerous colleagues, whose names are cited below, for their essential contributions to the work described here.

■ REFERENCES

(1) Kim, M. G.; Kanatzidis, M. G.; Facchetti, A.; Marks, T. J. Low-temperature fabrication of high-performance metal oxide thin-film electronics via combustion processing. *Nat. Mater.* **2011**, *10*, 382−388.

(2) Yu, X.; Smith, J.; Zhou, N. J.; Zeng, L.; Guo, P. J.; Xia, Y.; Alvarez, A.; Aghion, S.; Lin, H.; Yu, J. S.; Chang, R. P. H.; Bedzyk, M. J.; Ferragut, R.; Marks, T. J.; Facchetti, A. Spray-combustion synthesis: Efficient solution route to high-performance oxide transistors. *P. Natl. Acad. Sci. U. S. A.* **2015**, *112*, 3217−3222.

(3) Wang, B.; Guo, P.; Zeng, L.; Yu, X.; Sil, A.; Huang, W.; Leonardi, M. J.; Zhang, X.; Wang, G.; Lu, S.; Chen, Z.; Bedzyk, M. J.; Schaller, R. D.; Marks, T. J.; Facchetti, A. Expeditious, scalable solution growth of metal oxide films by combustion blade coating for flexible electronics. *P. Natl. Acad. Sci. U. S. A.* **2019**, *116*, 9230−9238.

(4) Huang, W.; Chien, P. H.; McMillen, K.; Patel, S.; Tedesco, J.; Zeng, L.; Mukherjee, S.; Wang, B.; Chen, Y.; Wang, G.; Wang, Y.; Gao, Y.; Bedzyk, M. J.; DeLongchamp, D. M.; Hu, Y. Y.; Medvedeva, J. E.; Marks, T. J.; Facchetti, A. Experimental and theoretical evidence for hydrogen doping in polymer solution-processed indium gallium oxide. *P. Natl. Acad. Sci. U. S. A.* **2020**, *117*, 18231−18239.

(5) Yu, X. G.; Marks, T. J.; Facchetti, A. Metal oxides for optoelectronic applications. *Nat. Mater.* **2016**, *15*, 383−396.

(6) Wang, B.; Huang, W.; Chi, L.; Al-Hashimi, M.; Marks, T. J.; Facchetti, A. High-*k* Gate Dielectrics for Emerging Flexible and Stretchable Electronics. *Chem. Rev.* **2018**, *118*, 5690−5754.

(7) Wang, B.; Zeng, L.; Huang, W.; Melkonyan, F. S.; Sheets, W. C.; Chi, L.; Bedzyk, M. J.; Marks, T. J.; Facchetti, A. Carbohydrate-Assisted Combustion Synthesis To Realize High-Performance Oxide Transistors. *J. Am. Chem. Soc.* **2016**, *138*, 7067−7074.

(8) Nomura, K.; Ohta, H.; Takagi, A.; Kamiya, T.; Hirano, M.; Hosono, H. Room-temperature fabrication of transparent flexible

thin-film transistors using amorphous oxide semiconductors. *Nature* **2004**, *432*, 488−492.
(9) Yao, Y.; Huang, W.; Chen, J. H.; Wang, G.; Chen, H. M.; Zhuang, X. M.; Ying, Y. B.; Ping, J. F.; Marks, T. J.; Facchetti, A. Flexible complementary circuits operating at sub-0.5 V via hybrid organic inorganic electrolyte-gated transistors. *P. Natl. Acad. Sci. U. S. A.* **2021**, *118*, No. e2111790118.
(10) Bang, H.-J.; Nguyen, M.-C.; Lee, D.-H.; Nguyen, A. H. T.; Kang, S.; Choi, J.-W.; Han, S. Y.; Choi, R. Effect of High Pressure Hydrogen or Deuterium Anneal on Polysilicon Channel Field Effect Transistors. *J. Nanosci. Nanotechnol.* **2016**, *16*, 10341−10345.
(11) Oh, S.-M.; Jo, K.-W.; Cho, W.-J. High performance solution-deposited bilayer channel indium-zinc-oxide thin film transistors by low-temperature microwave annealing. *Curr. Appl. Phys.* **2015**, *15*, S69−S74.
(12) Kim, W.-G.; Tak, Y. J.; Du Ahn, B.; Jung, T. S.; Chung, K.-B.; Kim, H. J. High-pressure Gas Activation for Amorphous Indium-Gallium-Zinc-Oxide Thin-Film Transistors at 100 °C. *Sci. Rep.* **2016**, *6*, 23039.
(13) Bashir, A.; Wobkenberg, P. H.; Smith, J.; Ball, J. M.; Adamopoulos, G.; Bradley, D. D. C.; Anthopoulos, T. D. High-Performance Zinc Oxide Transistors and Circuits Fabricated by Spray Pyrolysis in Ambient Atmosphere. *Adv. Mater.* **2009**, *21*, 2226−2231.
(14) Lin, Y. H.; Faber, H.; Zhao, K.; Wang, Q. X.; Amassian, A.; McLachlan, M.; Anthopoulos, T. D. High-Performance ZnO Transistors Processed Via an Aqueous Carbon-Free Metal Oxide Precursor Route at Temperatures Between 80−180 degrees C. *Adv. Mater.* **2013**, *25*, 4340−4346.
(15) Kim, H.; Ng, T. N. Reducing Trap States in Printed Indium Zinc Oxide Transistors by Doping with Benzyl Viologen. *Adv. Electron. Mater.* **2018**, *4*, 1700631.
(16) Kim, Y. H.; Heo, J. S.; Kim, T. H.; Park, S.; Yoon, M. H.; Kim, J.; Oh, M. S.; Yi, G. R.; Noh, Y. Y.; Park, S. K. Flexible metal-oxide devices made by room-temperature photochemical activation of sol-gel films. *Nature* **2012**, *489*, 128−132.
(17) Banger, K. K.; Yamashita, Y.; Mori, K.; Peterson, R. L.; Leedham, T.; Rickard, J.; Sirringhaus, H. Low-temperature, high-performance solution-processed metal oxide thin-film transistors formed by a 'sol-gel on chip' process. *Nat. Mater.* **2011**, *10*, 45−50.
(18) Hosono, H. How we made the IGZO transistor. *Nat. Electron.* **2018**, *1*, 428.
(19) Chen, R.; Lan, L. Solution-processed metal-oxide thin-film transistors: a review of recent developments. *Nanotechnology* **2019**, *30*, 312001.
(20) Xu, W.; Li, H.; Xu, J. B.; Wang, L. Recent Advances of Solution-Processed Metal Oxide Thin-Film Transistors. *ACS Appl. Mater. Interfaces* **2018**, *10*, 25878−25901.
(21) Carlos, E.; Martins, R.; Fortunato, E.; Branquinho, R. Solution Combustion Synthesis: Towards a Sustainable Approach for Metal Oxides. *Chem. Eur. J.* **2020**, *26*, 9099−9125.
(22) Yang, J.; Wang, B.; Zhang, Y.; Ding, X.; Zhang, J. Low-temperature combustion synthesis and UV treatment processed p-type Li:NiOx active semiconductors for high-performance electronics. *J. Mater. Chem. C* **2018**, *6*, 12584−12591.
(23) Liu, A.; Zhu, H.; Guo, Z.; Meng, Y.; Liu, G.; Fortunato, E.; Martins, R.; Shan, F. Solution Combustion Synthesis: Low-Temperature Processing for p-Type Cu:NiO Thin Films for Transparent Electronics. *Adv. Mater.* **2017**, *29*, 1701599.
(24) Zhang, X.; Wang, B.; Huang, W.; Chen, Y.; Wang, G.; Zeng, L.; Zhu, W.; Bedzyk, M. J.; Zhang, W.; Medvedeva, J. E.; Facchetti, A.; Marks, T. J. Synergistic Boron Doping of Semiconductor and Dielectric Layers for High-Performance Metal Oxide Transistors: Interplay of Experiment and Theory. *J. Am. Chem. Soc.* **2018**, *140*, 12501−12510.
(25) Luo, Y.-R.: *Comprehensive Handbook of Chemical Bond Energies*; CRC Press: Boca Raton, 2007.
(26) Hennek, J. W.; Smith, J.; Yan, A.; Kim, M. G.; Zhao, W.; Dravid, V. P.; Facchetti, A.; Marks, T. J. Oxygen "getter" effects on microstructure and carrier transport in low temperature combustion-processed a-InXZnO (X = Ga, Sc, Y, La) transistors. *J. Am. Chem. Soc.* **2013**, *135*, 10729−10741.
(27) Smith, J.; Zeng, L.; Khanal, R.; Stallings, K.; Facchetti, A.; Medvedeva, J. E.; Bedzyk, M. J.; Marks, T. J. Cation Size Effects on the Electronic and Structural Properties of Solution-Processed In-X-O Thin Films. *Adv. Electron. Mater.* **2015**, *1*, 1500146.
(28) Wang, B.; Yu, X.; Guo, P.; Huang, W.; Zeng, L.; Zhou, N.; Chi, L.; Bedzyk, M. J.; Chang, R. P. H.; Marks, T. J.; Facchetti, A. Solution-Processed All-Oxide Transparent High-Performance Transistors Fabricated by Spray-Combustion Synthesis. *Adv. Electron. Mater.* **2016**, *2*, 1500427.
(29) Yang, W.; Wang, H.; Zhang, M.; Zhu, J.; Zhou, J.; Wu, S. Fuel properties and combustion kinetics of hydrochar prepared by hydrothermal carbonization of bamboo. *Bioresour. Technol.* **2016**, *205*, 199−204.
(30) Martin, R. B. Metal ion stabilities correlate with electron affinity rather than hardness or softness. *Inorganica. Chim.* **1998**, *283*, 30−36.
(31) Wang, B.; Leonardi, M. J.; Huang, W.; Chen, Y.; Zeng, L.; Eckstein, B. J.; Marks, T. J.; Facchetti, A. Marked Cofuel Tuning of Combustion Synthesis Pathways for Metal Oxide Semiconductor Films. *Adv. Electron. Mater.* **2019**, *5*, 1900540.
(32) Curl, R. L. Handbook of Environmental Data on Organic-Chemicals, 2nd Edition - Verschueren,K. *J. Am. Chem. Soc.* **1984**, *106*, 830.
(33) Levine, M.; DiScenza, D. J. Sweet, Sweet Science: Addressing the Gender Gap in STEM Disciplines through a One-Day High School Program in Sugar Chemistry. *J. Chem. Educ.* **2018**, *95*, 1316−1322.
(34) Goll, J. G.; Wilkinson, L. J.; Snell, D. M. Teaching Chemistry Using October Sky. *J. Chem. Educ.* **2009**, *86*, 177−180.
(35) Zhuang, X.; Patel, S.; Zhang, C.; Wang, B.; Chen, Y.; Liu, H.; Dravid, V. P.; Yu, J.; Hu, Y. Y.; Huang, W.; Facchetti, A.; Marks, T. J. Frequency-Agile Low-Temperature Solution-Processed Alumina Dielectrics for Inorganic and Organic Electronics Enhanced by Fluoride Doping. *J. Am. Chem. Soc.* **2020**, *142*, 12440−12452.
(36) Sil, A.; Avazpour, L.; Goldfine, E. A.; Ma, Q.; Huang, W.; Wang, B.; Bedzyk, M. J.; Medvedeva, J. E.; Facchetti, A.; Marks, T. J. Structure-Charge Transport Relationships in Fluoride-Doped Amorphous Semiconducting Indium Oxide: Combined Experimental and Theoretical Analysis. *Chem. Mater.* **2020**, *32*, 805−820.
(37) Yu, X.; Zeng, L.; Zhou, N.; Guo, P.; Shi, F.; Buchholz, D. B.; Ma, Q.; Yu, J.; Dravid, V. P.; Chang, R. P.; Bedzyk, M.; Marks, T. J.; Facchetti, A. Ultra-flexible, "invisible" thin-film transistors enabled by amorphous metal oxide/polymer channel layer blends. *Adv. Mater.* **2015**, *27*, 2390−2399.
(38) Huang, W.; Zeng, L.; Yu, X. G.; Guo, P. J.; Wang, B. H.; Ma, Q.; Chang, R. P. H.; Yu, J. S.; Bedzyk, M. J.; Marks, T. J.; Facchetti, A. Metal Oxide Transistors via Polyethylenimine Doping of the Channel Layer: Interplay of Doping, Microstructure, and Charge Transport. *Adv. Funct. Mater.* **2016**, *26*, 6179−6187.
(39) Huang, W.; Guo, P.; Zeng, L.; Li, R.; Wang, B.; Wang, G.; Zhang, X.; Chang, R. P. H.; Yu, J.; Bedzyk, M. J.; Marks, T. J.; Facchetti, A. Metal Composition and Polyethylenimine Doping Capacity Effects on Semiconducting Metal Oxide-Polymer Blend Charge Transport. *J. Am. Chem. Soc.* **2018**, *140*, 5457−5473.
(40) Wang, Z.; Zhuang, X.; Wang, B.; Huang, W.; Marks, T. J.; Facchetti, A. Doping Indium Oxide Films with Amino-Polymers of Varying Nitrogen Content Markedly Affects Charge Transport and Mechanical Flexibility. *Adv. Funct. Mater.* **2021**, *31*, 2100451.
(41) Chen, Y.; Huang, W.; Sangwan, V. K.; Wang, B.; Zeng, L.; Wang, G.; Huang, Y.; Lu, Z.; Bedzyk, M. J.; Hersam, M. C.; Marks, T. J.; Facchetti, A. Polymer Doping Enables a Two-Dimensional Electron Gas for High-Performance Homojunction Oxide Thin-Film Transistors. *Adv. Mater.* **2019**, *31*, No. e1805082.
(42) Faber, H.; Das, S.; Lin, Y. H.; Pliatsikas, N.; Zhao, K.; Kehagias, T.; Dimitrakopulos, G.; Amassian, A.; Patsalas, P. A.; Anthopoulos, T. D. Heterojunction oxide thin-film transistors with unprecedented electron mobility grown from solution. *Sci. Adv.* **2017**, *3*, No. e1602640.

https://doi.org/10.1021/acs.accounts.1c00671
Acc. Chem. Res. 2022, 55, 429−441

(43) Lee, S.; Ghaffarzadeh, K.; Nathan, A.; Robertson, J.; Jeon, S.; Kim, C.; Song, I. H.; Chung, U. I. Trap-limited and percolation conduction mechanisms in amorphous oxide semiconductor thin film transistors. *Appl. Phys. Lett.* **2011**, *98*, 203508.
(44) Benco, L.; Tunega, D.; Hafner, J.; Lischka, H. Upper Limit of the O-H···O Hydrogen Bond. Ab Initio Study of the Kaolinite Structure. *J. Phys. Chem. B* **2001**, *105*, 10812−10817.
(45) Huang, W.; Wang, G.; Luo, C.; Xu, Y.; Xu, Y.; Eckstein, B. J.; Chen, Y.; Wang, B.; Huang, J.; Kang, Y.; Wu, J.; Dravid, V. P.; Facchetti, A.; Marks, T. J. Controllable growth of LiMn2O4 by carbohydrate-assisted combustion synthesis for high performance Li-ion batteries. *Nano Energy* **2019**, *64*, 103936.
(46) Zheng, D.; Wang, G.; Huang, W.; Wang, B.; Ke, W.; Logsdon, J. L.; Wang, H.; Wang, Z.; Zhu, W.; Yu, J.; Wasielewski, M. R.; Kanatzidis, M. G.; Marks, T. J.; Facchetti, A. Combustion Synthesized Zinc Oxide Electron-Transport Layers for Efficient and Stable Perovskite Solar Cells. *Adv. Funct. Mater.* **2019**, *29*, 1900265.
(47) Baeg, K. J.; Kim, M. G.; Song, C. K.; Yu, X.; Facchetti, A.; Marks, T. J. Charge-trap flash-memory oxide transistors enabled by copper-zirconia composites. *Adv. Mater.* **2014**, *26*, 7170−7177.
(48) Wang, B.; Thukral, A.; Xie, Z.; Liu, L.; Zhang, X.; Huang, W.; Yu, X.; Yu, C.; Marks, T. J.; Facchetti, A. Flexible and Stretchable Metal Oxide Nanofiber Networks for Multimodal and Monolithically Integrated Wearable Electronics. *Nat. Commun.* **2020**, *11*, 2405.

https://doi.org/10.1021/acs.accounts.1c00671
Acc. Chem. Res. 2022, 55, 429−441